Three-dimensional Crack Tip Deformation Measurement Using Combined Moiré-Sagnac Interferometry

by B. S.-J. Kang and S. M. Anderson

ABSTRACT—A combined Moiré-Sagnac interferometry method is developed for in-plane (u and v) and out-of-plane (w) surface deformation measurement. The combined optical setup is used to measure three-dimensional crack tip deformations of Al 2024-0 and Al 2024-T4 specimens at room temperature and an Inconel 909 specimen at 570°C. Measured displacements near the crack tip region of the Al 2024-T4 specimen are used as input nodal displacements to determine stress intensity factors based on two-dimensional and three-dimensional Jacobian derivative method. The values compare favorably with theoretical calculations. The extent of the three-dimensional crack tip deformation zone is also discussed.

KEY WORDS—3-D crack-tip deformation, Moiré-Sagnac Interferometry, high-temperature measurement, Jacobian Derivative method

Three-dimensional crack tip displacement measurements are often needed in the field of fracture mechanics research. The crack tip region may be subjected to large deformation gradients, and typical experimental methods, which can only measure discrete surface deformations, may not provide sufficient information about the deformations in this region. Acquiring crack tip displacements becomes even more complicated when the measurements are made under harsh environmental conditions such as under high temperatures. In these instances, it may not be possible or desirable to affix a measuring device to the specimen. As an alternative, various optical techniques have been developed to measure surface deformations. These optical techniques provide full-field measurements. The response time is essentially instantaneous, and the measurement system does not interfere with the process examined.

Moiré interferometry has been shown to be applicable for in-plane deformation measurement of specimens under harsh environmental conditions, i.e., at elevated temperatures[1–4] or in liquid medium.[5] To obtain out-of-plane displacements, techniques such as Michelson interferometry, moiré interferometry and holographic interferometry have been employed, but only under stable environments, e.g., room temperature.[6–10] Measurements obtained by Michelson interferometry or similar interferometric methods are sensitive to variations in the medium (such as temperature field fluctuation and flatness of the furnace window) and thus may not be suitable for high-temperature testing. Moiré interferometry can be used to measure both in-plane and out-of-plane displacements;[8,9] however, the approach requires the placement of a reference grating near the surface of the specimen to measure the out-of-plane displacements. This configuration is not practical for a specimen under elevated temperature conditions. The technique of holographic interferometry requires the superposition of a deformed image onto an original undeformed image[6] and thus is sensitive to the stability of the mechanical system and environmental conditions.[10] A simpler method for obtaining the out-of-plane displacements is desired.

The purpose of this paper is to report the development of a combined optical method capable of full-field three-dimensional surface displacement measurements of specimens under elevated temperature conditions. Moiré interferometry is used to obtain the in-plane displacements, and an application involving Sagnac interferometry, which was presented in 1913 as a method for measuring angular velocities, is developed for measuring the out-of-plane surface deformations. Both interferometric techniques give full-field measurements and do not require physical contact with the specimen. This combined method has been used to measure the crack tip deformations in single-edge-notched tension (SENT) specimens of different materials and under different environmental conditions. The three-dimensional crack tip deformation fields obtained from an Al 2024-T4 specimen are used as input boundary nodal displacements to determine the stress intensity factors based on two-dimensional and three-dimensional Jacobian derivative method (JDM).[11] Finally, out-of-plane deformation fields obtained in this approach are compared with theoretical predictions[12] and with previous results from an etching technique,[13] finite element analysis[14,15] and caustics.[16]

Sagnac Interferometry

The Sagnac interferometer (also referred to as a triangular-path macro-interferometer, an anti-resonant ring interferometer or a beam splitter interferometer) is an amplitude-splitting device that was used in 1913 by G. Sagnac to measure the angular velocity of a rotating system.[17] More recently, it has been used in applications such as fiber logic gates, laser gyroscopes and quasi-microwave junctions.[18,19] The main feature of this device is that the two beams present in the system

B. S.-J. Kang (SEM Member) is an Associate Professor, Department of Mechanical and Aerospace Engineering, West Virginia University, Morgantown, WV 26506. S. M. Anderson is a Cognizant Engineer, Plant Apparatus Division, Bechtel Plant Machinery Inc., Pittsburgh, PA 15235.

Original manuscript submitted: October 4, 1999.
Final manuscript received: October 23, 2000.

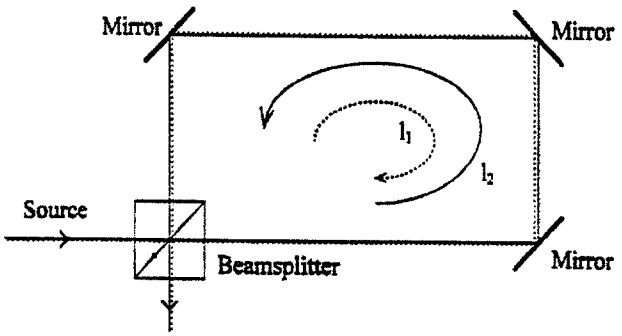

Fig. 1—Optical paths of a Sagnac interferometer

travel in identical but oppositely directed paths before they are recombined at the beam splitter.

The Sagnac interferometer is similar to a Michelson interferometer, but the initial null field (i.e., no fringes) is always achieved irrespective of the initial specimen surface warping. An example of a three-mirror Sagnac interferometer is shown in Fig. 1. A collimated wave front is first divided by a beam splitter into two wave fronts with the same waveform. Each waveform is then directed around an identical closed path in opposite directions and then recombined at the beam splitter. This initial alignment produces a null field from the interference between the recombining wave fronts, since both have the same wave shape and pathlength. When one of the mirrors is subjected to a translational shift (dh, dv), an optical path difference (dl) between the two wave fronts is formed, i.e.,

$$dl = 2(dv - dh). \tag{1}$$

For a purely translational shift, dv is equivalent to dh and dl becomes zero. This corresponds to rigid-body translational, and no interferometric fringe will be generated. However, for a rotation of one of the mirrors by an angle θ, the recombining wave fronts will intersect at an angle of 2θ and form interferometric fringes; i.e., for a surface that rotates an angle θ, the corresponding out-of-plane displacement can be represented by

$$w = \frac{N\lambda}{2}, \tag{2}$$

where λ is the wavelength of the light source and N is the fringe order. This optical setup is insensitive to rigid-body translation and to the initial surface warping of the mirrors; however, displacements resulting from rigid-body rotation of one of the surfaces will cause fringe formation.

Note that the three-mirror setup will generate a transposed image, as shown in Fig. 2(a); therefore, for the experimental work presented in this paper, a four-mirror Sagnac interferometer was adopted such that the two recombined images will superimpose onto each other at identical input locations, as illustrated in Fig. 2(b). As also shown in Fig. 2(b), one of the four mirrors of the Sagnac interferometer is replaced by the specimen and the remaining mirrors are fixed; thus, any fringe pattern produced will be due to surface deformations of the specimen.

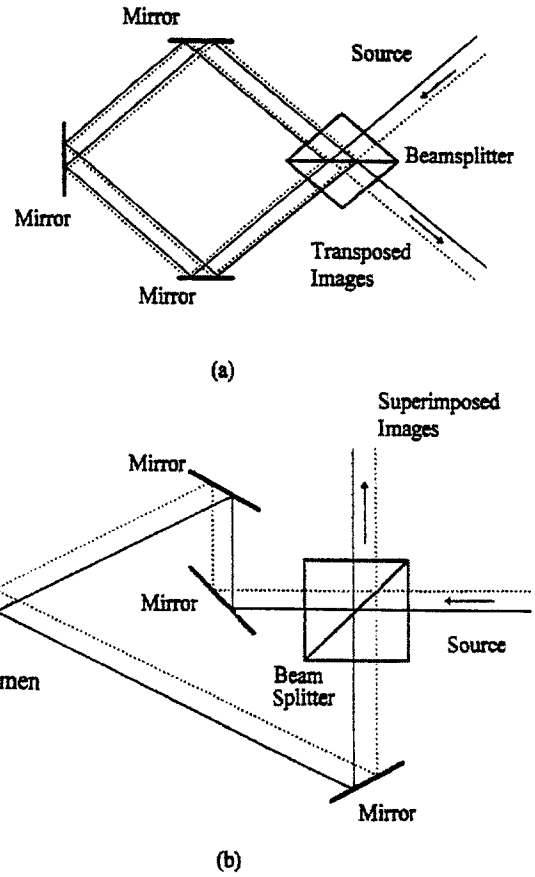

Fig. 2—Images acquired from a (a) three-mirror Sagnac interferometer and (b) four-mirror Sagnac interferometer

Experimental Program

SENT specimens made of Al 2024-0, Al 2024-T4 and Inconel 909 were tested using the combined moiré-Sagnac interferometry method. The general configuration of the specimens is shown in Fig. 3. In each specimen, an initial saw cut crack was made using a thin diamond-edge saw blade. After the cut, the Al 2024-T4 and Inconel 909 specimens were fatigue-precracked, with the maximum cyclic load corresponding to 15 percent of the fracture toughness value of the material.

Specimen Grating

Once the initial crack was generated, the cross-lined grating necessary for moiré interferometry was applied to each specimen. For the tests conducted at room temperature, 600 lines/mm cross-lined grating was transformed onto the specimen using PC-6C adhesive (Measurements Group Inc.) following standard moiré grating transfer procedure.[20] However, for tests conducted at elevated temperatures, a special grating transfer procedure[1] was applied to chemically etch a 300 line/mm cross-lined pattern onto the Inconel 909 specimen surface, i.e., zero-thickness specimen grating.

Optical Setup

Figure 4 shows the combined moiré-Sagnac interferometry optical setup for conducting tests to record the three-dimensional full-field crack tip deformations. The Sagnac

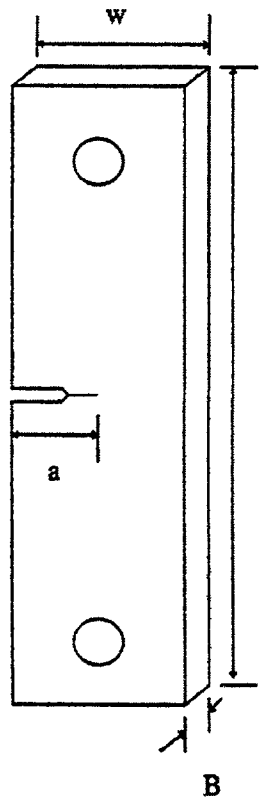

	a	w	B	h
Al2024-0	14	25	0.8	140
Al2024-T4	8.6	19	3.2	140
Inconel909	9.0	25	1.7	140

unit = mm

Fig. 3—Test specimen geometry

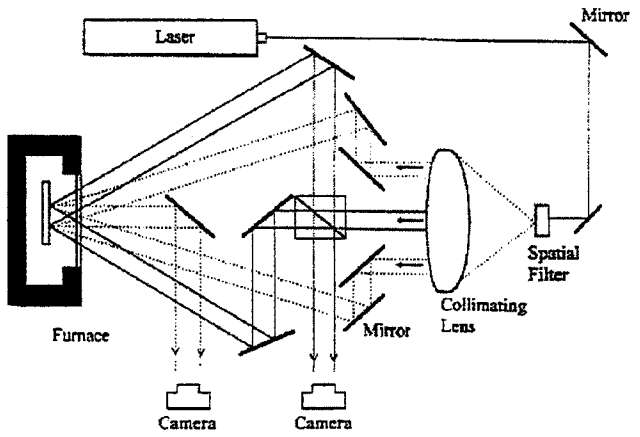

Fig. 4—Optical setup for combined moiré-Sagnac interferometry (dotted line = moiré interferometry, solid line = Sagnac interferometry)

interferometry component is shown with a solid line, and the moiré interferometry component is shown with a dotted line. The specimen, which is mounted on a loading frame, and the entire optical setup, excluding the recording device, is assembled on an optical isolation table. The Inconel 909 specimen is mounted inside a furnace that is also mounted on the optical table. Previous work[2,5] has shown that the window required to be placed in the optical path for the high-temperature testing has no effect on the in-plane moiré fringe patterns produced. The optical setup consists of a 200 mW argon ion laser, a spatial filter, a collimating lens, a beam splitter and several mirrors used as beam-directing elements. The collimated light that passes through the center portion of the collimating lens is used for the Sagnac interferometer. The collimated light from the outer edges of the collimating lens is used for the moiré interferometry setup (dotted lines), which has been described in several publications.[4,20,21]

The images produced by the moiré and Sagnac interferometry setups were recorded using two 35 mm cameras (one to record the u and v displacement fields and the other for the w displacement field) with Kodak T-Max 3200 black-and-white film.

Results and Discussion

Large-scale Deformation Fields

To demonstrate that for a thin specimen the moiré-Sagnac interferometer can record the shear-lips characteristic of a plane stress ductile specimen, an Al 2024-0 specimen of 0.8 mm thickness was tested. This material was chosen for its strain-hardening behavior with large out-of-plane deformation at the crack tip region. The specimen was loaded incrementally to initiate stable crack growth leading to final failure, and the corresponding fringe patterns were recorded. Figures 5 and 6 illustrate the progression of displacement fields from small-scale yielding to large-scale yielding. The shear-lips, clearly visible in Fig. 6, can be compared to the theoretical predictions[12,22] under the plane stress condition and to previous experiments performed by Hahn and Rosenfield.[13]

High-temperature Testing

The feasibility of applying the combined moiré-Sagnac interferometry technique for the three-dimensional surface deformation measurement of specimens at elevated temperatures was demonstrated using an Inconel 909 specimen. This specimen was first placed in the furnace, and then the furnace temperature was increased incrementally to 570°C; this process took about 1 h to complete. A constant load of 4048 N was then applied to the specimen. Figures 7 and 8 show the specimen under constant load at $t = 0$ min and $t = 300$ min, respectively. As can be seen in Fig. 7, some amount of specimen surface oxidation has already been formed at this testing stage. Figure 8 shows that much more surface oxidation accumulated and the contrast of the moiré fringes further deteriorated. Subsequent photos became even more difficult to analyze; thus, for Inconel 909 at 570°C, the testing period is limited. However, for materials that do not exhibit such extensive oxidation, such as Inconel 718, the testing time can be increased significantly (over one week[3,4]).

K_I Evaluation Using JDM

An Al 2024-T4 specimen was tested to provide three-dimensional crack tip surface deformations to be used as input for an algorithm based on JDM.[11] This material was used as an elastic perfectly plastic material. The fringe patterns were obtained corresponding to a number of incrementally applied loads. Figure 9 shows one such set of fringes under an applied load of 3848 N. Also shown in the figure

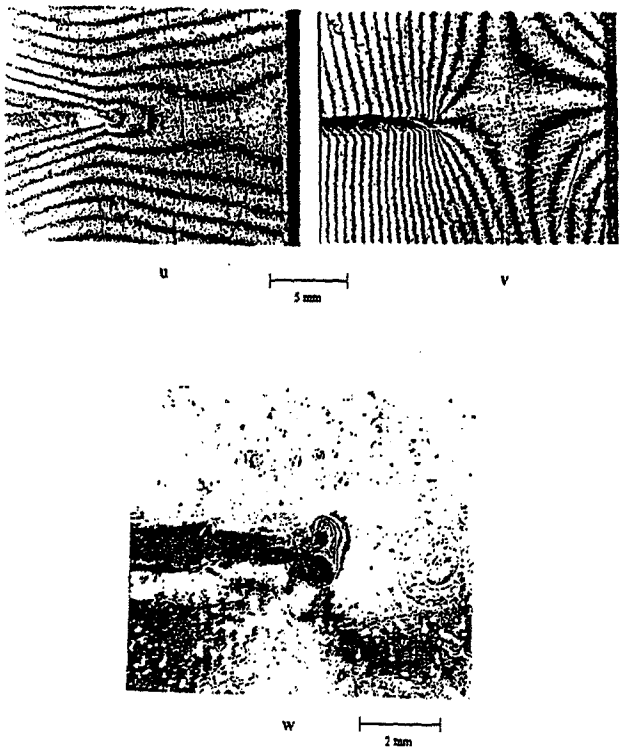

Fig. 5—Three-dimensional displacement fields for Al 2024-0 specimen at $P = 311$ N

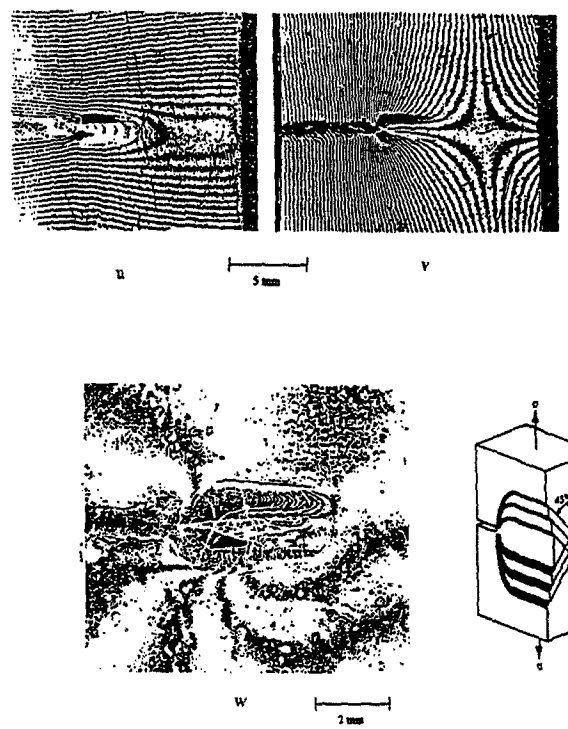

Fig. 6—Three-dimensional displacement fields for Al 2024-0 specimen at $P = 547$ N

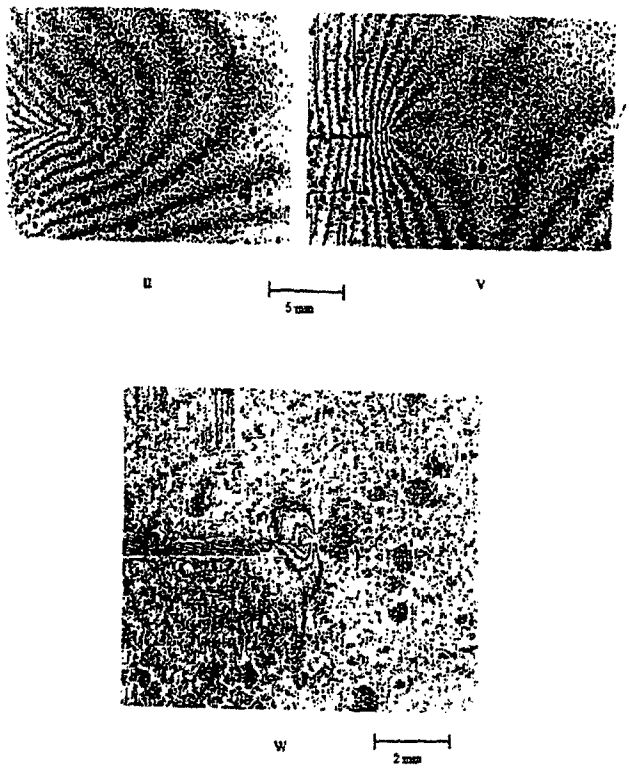

Fig. 7—Three-dimensional displacement fields for Inconel 909 specimen at $P = 4048$ N and $t = 0$ min

are the superimposed meshes that were used to obtain nodal displacement values for calculating mode I stress intensity factors using JDM.

JDM, which was proposed by Barbero and Reddy,[11] is a method for computing the strain energy release rate (G). The derivation of JDM is an extension of virtual crack extension method (VCEM)[23] and the stiffness derivative method.[24] As in VCEM, the strain energy release rate is computed from the formula

$$G = \frac{\partial U}{\partial a}, \tag{3}$$

where U is the strain energy and a is the crack length. The theoretical formulation presented by Barbero and Reddy provides the following expression for the strain energy release rate

$$G = \frac{1}{2}\sum u^T \int_{\Omega_e} \left[\left(\dot{B}^T D B - B^T D \dot{B}\right)|J| + B^T D B \frac{\partial |J|}{\partial a}\right] dr\, ds\, u, \tag{4}$$

where $\mathbf{u}$ is the vector of nodal displacements, $\mathbf{B}$ is the strain-displacement matrix, $\mathbf{D}$ is the constitutive matrix, Ω_e is the domain, e is the number of elements connected to the crack tip and

$$\dot{B} = \left[J^{-1}\frac{\partial J}{\partial a} B\right]. \tag{5}$$

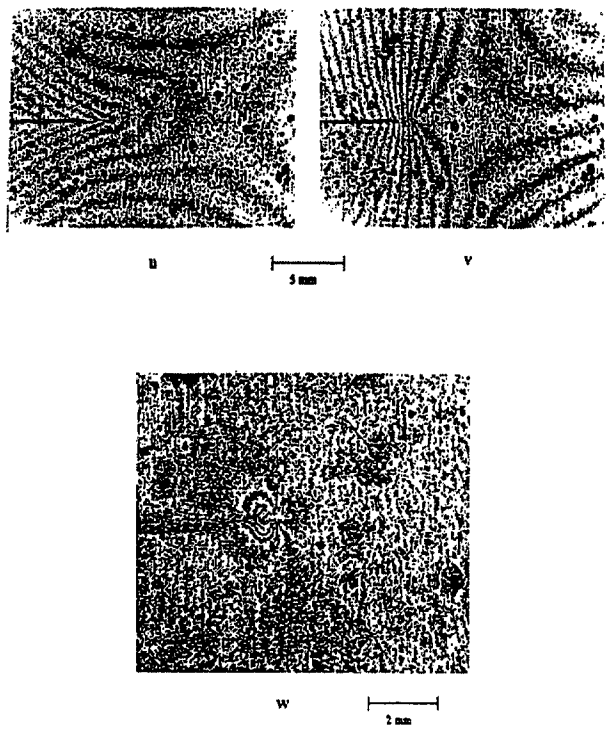

Fig. 8—Three-dimensional displacement fields for Inconel 909 specimen at $P = 4048$ N and $t = 300$ min

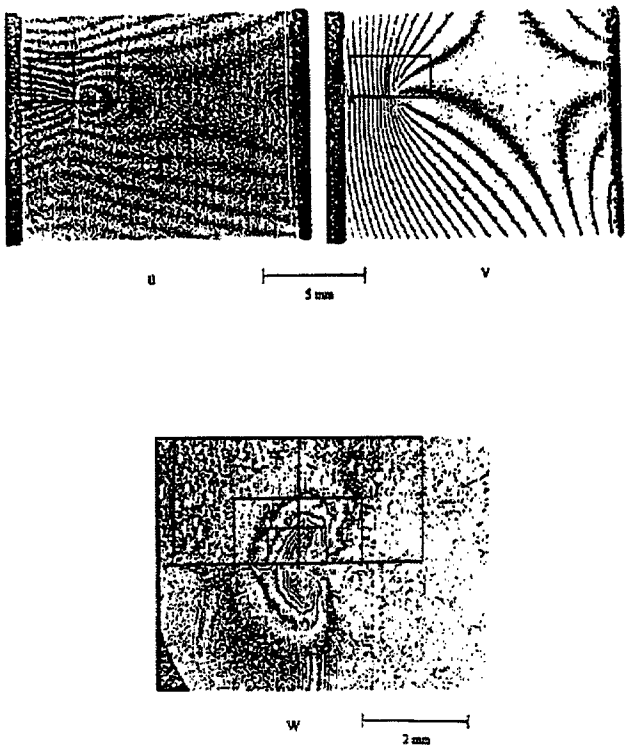

Fig. 9—Three-dimensional displacement fields for Al 2024-T4 specimen at $P = 3848$ N (mesh with d/B ratio of .65 superimposed on the u and v fields, and meshes with d/B ratios of .1625, .325 and .65 superimposed on the w field

The derivatives of the Jacobian are computed by the formula

$$\frac{\partial J}{\partial a} = \begin{bmatrix} \sum \Phi_{i,r} \frac{\partial x_i}{\partial a} & \sum \Phi_{i,r} \frac{\partial y_i}{\partial a} & \sum \Phi_{i,r} \frac{\partial z_i}{\partial a} \\ \sum \Phi_{i,s} \frac{\partial x_i}{\partial a} & \sum \Phi_{i,s} \frac{\partial y_i}{\partial a} & \sum \Phi_{i,s} \frac{\partial z_i}{\partial a} \\ \sum \Phi_{i,t} \frac{\partial x_i}{\partial a} & \sum \Phi_{i,t} \frac{\partial y_i}{\partial a} & \sum \Phi_{i,t} \frac{\partial z_i}{\partial a} \end{bmatrix}, \quad (6)$$

where (r, s, t) are local coordinates of the isoparametric element Φ_i, (x_I, y_I, z_I) are global coordinates of the elements and vector

$$v = \left(\frac{\partial x_i}{\partial a} \quad \frac{\partial y_i}{\partial a} \quad \frac{\partial z_i}{\partial a} \right) \quad (7)$$

indicates the direction and shape of the virtual crack extension.

Note that with JDM, it is not necessary to assign an arbitrary crack extension to the specimen as with VCEM, since JDM calculates G from eq (4) exactly. However, evaluation of eq (4) requires the nodal displacements of two elements surrounding the crack tip. These nodal displacements can either be two-dimensional in-plane displacements with the added constraint of either plane stress or plane strain or three-dimensional with no added constraint. Typical two-dimensional and three-dimensional meshes are shown in Fig. 10. In these diagrams, d is the dimension of the elements and B is the thickness of the specimen. Two-dimensional and three-dimensional JDM computer codes were obtained from Barbero.[25]

Analysis of the Al 2024-T4 specimen was done using both two-dimensional and three-dimensional JDM. For the two-dimensional case, plane stress was assumed. As typically shown in Fig. 9, a mesh with a d/B ratio of 0.65 is shown superimposed on the u and v displacement fields, and meshes with d/B ratios of 0.1625, 0.325 and 0.65 are superimposed on the w displacement field. Displacement values were assumed symmetric for both specimen surfaces in the three-dimensional case. Elements with d/B ratios of 0.1625, 0.325 and 0.65 were applied to the displacement data for $P = 2055$ N, $P = 3100$ N and $P = 3848$ N, respectively, to obtain strain energy release rates (G) for each case, which were converted to stress intensity factor (K_I) using the relation

$$K_I = \sqrt{GE}, \quad (8)$$

where E is Young's modulus.

Stress intensity factors obtained from two-dimensional and three-dimensional JDM were compared with each other and also with theoretical calculations.[26] The comparison of the stress intensity factors given in Tables 1 and 2 shows that the two-dimensional and three-dimensional cases have the best correlation as the element size increases. Three-dimensional JDM is within 1.2 percent of the theoretical value for each of the loading cases for a d/B ratio of 0.65, compared with a maximum difference of 14.2 percent for the two-dimensional case. As the elements become smaller, both the two-dimensional and three-dimensional methods produce stress intensive factors that are significantly different from the theoretical values, with the two-dimensional case producing a larger percentage difference. This should be the case because the assumption of plane stress becomes less valid (i.e.,

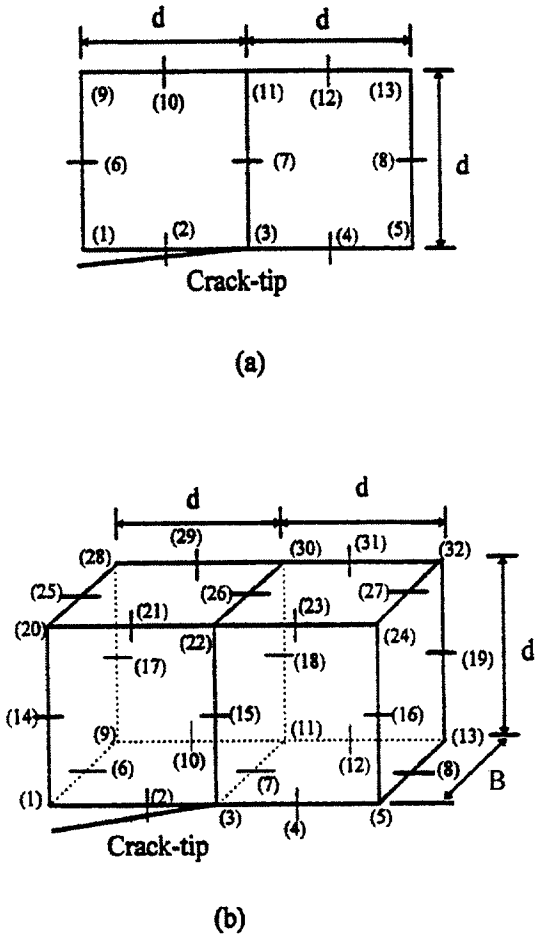

Fig. 10—Schematic of mesh applied for (a) two-dimensional Jacobian derivative method and (b) three-dimensional Jacobian derivative method

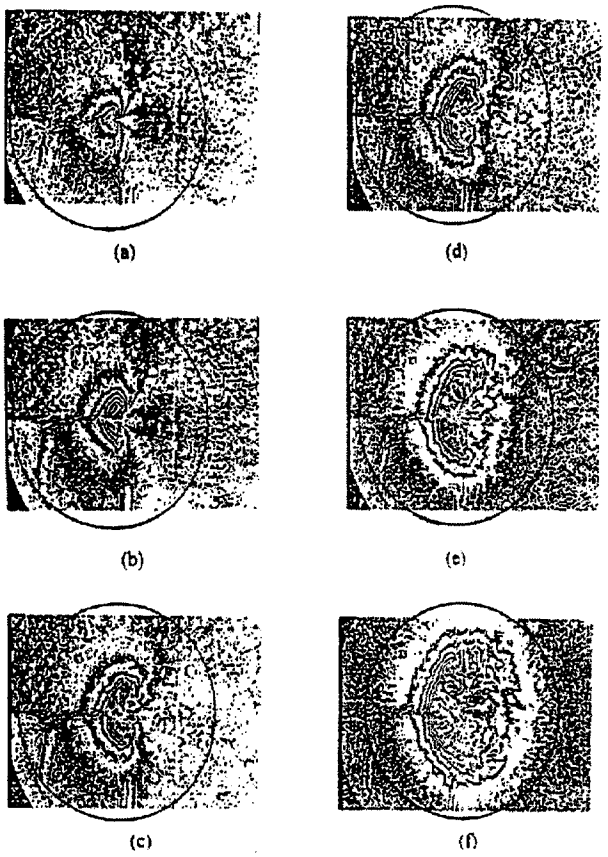

Fig. 11—Radius of 0.7 times the specimen thickness (3.2 mm) superimposed on w displacement fields of an Al 2024-T4 specimen for loads of (a) 2055 N, (b) 3100 N, (c) 3848 N, (d) 4088 N, (e) 4617 N and (f) 5129 N

closer to the crack tip). As would be expected, the largest percentage error is for the case of highest loading and with the smallest d/B ratio, where the elements are dominated by the three-dimensional crack tip plastic deformation. Therefore, application of JDM should be restricted to mesh nodal points sufficiently away from the crack tip region where the assumption of linear elastic deformation is valid. Based on the results shown in Tables 1 and 2, we suggest the use of a mesh size larger than a d/B ratio of 0.65 for two-dimensional JDM and a mesh size from a d/B ratio 0.33 to a d/B ratio of 0.65 for three-dimensional JDM. This technique has been previously compared to the crack closure technique,[11] and it has been shown that the solution from the crack closure technique approaches the two-dimensional JDM solution. Therefore, three-dimensional JDM should provide more accurate stress intensity factor values compared with the crack closure technique. Note that application of three-dimensional JDM should use elements that are on the periphery of the three-dimensional crack tip region but outside of the crack tip process zone.

Comparison of Out-of-plane Displacements with Previous Investigations

Several investigators have attempted to determine the extent of the three-dimensional field in a crack tip region.[13–16] Through numerical calculations performed by Yang and Freund,[14] those investigators determined that the three-dimensional deformations were dominant within a region with a radius between 0.5 and 0.75 times the thickness of a specimen, and that outside this radius the deformations can be considered as under a plane stress condition. They also showed that within this region, the deformation field cannot be approximated by a plane strain solution. Finite element analysis performed by Nakamura and Parks[15] and experimental results by Rosakis and Ravi-Chandar[16] illustrate how the three-dimensional effect does occur within a radius of approximately 0.5 times the specimen thickness. Our results are in agreement with their findings. Figure 11 shows the w fields of the Al 2024-T4 specimen, where a circle of radius 0.7 times the specimen thickness is superimposed on the out-of-plane deformation fields for different loads. As shown, it can be seen that the radius of the three-dimensional deformation region increases rapidly as the load is increased but remains confined within a radius of about 0.5 times the specimen thickness, which correlates well with previous investigations.[14–16]

Conclusion

Based on the results presented in this paper, the following conclusions are drawn:

TABLE 1—STRESS INTENSITY FACTORS FOR VARYING d/B RATIOS (Al 2024-T4 SPECIMEN): (A) THREE-DIMENSIONAL JACOBIAN DERIVATIVE METHOD AND (B) TWO-DIMENSIONAL JACOBIAN DERIVATIVE METHOD

	Three-dimensional Jacobian Derivative Method (MPa$\sqrt{m}$)			
(A) Load	Contour 1 (d/B = 0.1625)	Contour 2 (d/B = 0.325)	Contour 3 (d/B = 0.65)	Theoretical
P = 2055 N	13.86	11.98	13.02	12.88
P = 3100 N	21.76	19.56	19.67	19.58
P = 3848 N	36.07	26.56	23.84	24.12
	Two-dimensional Jacobian Derivative Method (MPa$\sqrt{m}$)			
(B) Load	Contour 1 (d/B = 0.1625)	Contour 2 (d/B = 0.325)	Contour 3 (d/B = 0.65)	Theoretical
P = 2055 N	11.41	10.77	11.77	12.88
P = 3100 N	15.66	15.68	16.80	19.58
P = 3848 N	28.77	23.43	21.28	24.12

TABLE 2—PERCENTAGE DIFFERENCE BETWEEN EXPERIMENTAL AND THEORETICAL STRESS INTENSITY FACTORS: (A) THREE-DIMENSIONAL JACOBIAN DERIVATIVE METHOD AND (B) TWO-DIMENSIONAL JACOBIAN DERIVATIVE METHOD

	Three-dimensional Jacobian Derivative Method (percentage difference)		
(A) Load	Contour 1 (d/B = 0.1625)	Contour 2 (d/B = 0.325)	Contour 3 (d/B = 0.65)
P = 2055 N	7.61	6.99	1.09
P = 3100 N	11.13	0.10	0.46
P = 3848 N	49.54	10.12	1.16
Overall	22.76	5.74	0.90
	Two-dimensional Jacobian Derivative Method (percentage difference)		
(B) Load	Contour 1 (d/B = 0.1625)	Contour 2 (d/B = 0.325)	Contour 3 (d/B = 0.65)
P = 2055 N	10.41	16.38	8.62
P = 3100 N	20.02	19.91	14.20
P = 3848 N	19.28	2.86	11.77
Overall	16.57	13.05	11.53

- A combined moiré-Sagnac interferometry method is developed for in-plane (u and v) and out-of-plane (w) surface deformation measurement.
- Measurements of three-dimensional full-field crack tip deformations on SENT specimens of Al 2024-0, Al 2024-T4 and Inconel 909, under different testing conditions, demonstrate that this method is applicable for small-scale yielding and for large-scale yielding deformation measurement. Furthermore, this method is capable of three-dimensional deformation measurement of specimens under elevated temperature conditions.
- Good correlation between the experimental and theoretical stress intensity factors shows that two-dimensional and three-dimensional JDM can be successfully employed to obtain the stress intensity factors from the experimental data of two-dimensional and three-dimensional crack tip deformations.
- The extent of the three-dimensional crack tip field is discussed. Our experimental results are in agreement with previous investigations[14–16] that the three-dimensional crack tip region is confined to approximately 0.5 times the specimen thickness.

Acknowledgments

This work was supported by the West Virginia University/National Science Foundation EPSCOR (Experimental Program to Stimulate Competitive Research) Computational Materials Research Program.

References

1. Kang, B.S.J., Zhang, G.Z., Jenkins, M.G., Ferber, M., and Ifju, P., "Development of Moire-interferometry for In-situ Material Surface Deformation Measurement at High Temperature," SEM Spring Conference on Experimental Mechanics, Dearborn, Michigan, 964–976 (1993).

2. Wang, F.X., Ifju, P., and Kang, B.S.-J., "High-temperature Moire Interferometry Using Zero-thickness Grating," SEM Spring Conference on Experimental Mechanics, Las Vegas, Nevada, 727–731 (1992).

3. Kang, B.S.-J., Yao, Q., Li, Z., and Liu, C.T., "Investigation on Environmental Assisted Fracture Behavior of Iron Aluminides Using Moire Interferometry," Mat. Sci. Eng., **A239-240**, *344–352 (1997).*

4. Carpenter, W., Kang, B.S.-J., and Chang, K.M., "SAGBO Mechanism on High Temperature Cracking Behavior of Ni-base Superalloys," TMS International Symposium on Superalloys, 718, 625, 706 and Various Derivatives, Pittsburgh, Pennsylvania, 679–688 (1997).

5. Wang, F.X. and Kang, B.S.-J., "Moire Interferometry in Liquid Mediums," SEM, Proceedings of the VII International Congress on Experimental Mechanics, Las Vegas, Nevada, 1711–1766 (1992).

6. Vest, C.M., "Coherent Optics, Holography, and Holographic Interferometry," in Holographic Interferometry, John Wiley & Sons, New York, 1–66 (1979).

7. Hecht, E. and Zajac, A., Optics, Addison-Wesley, Reading, MA (1974).

8. Post, D., Han, B., and Ifju, P., High Sensitivity Moire, Springer-Verlag, New York (1994).

9. Asundi, A., Cheung, M.T., and Lee, C.S., "Moire Interferometry for Simultaneous Measurement of u, v, w," EXPERIMENTAL MECHANICS, **29**, *258–260 (1989).*

10. Daniel, I.M., "Experimental Methods in Applied Mechanics," J. Appl. Mech., **50**, *973–976 (1983).*

11. Barbero, E.J. and Reddy, J.N., "The Jacobian Derivative Method for Three-dimensional Fracture Mechanics," Communications Appl. Numer. Meth., **6**, *507–518 (1990).*

12. Edward, H.L. and Wanhill, R.J.H., "Crack-tip Plasticity," in Fracture Mechanics, Edward Arnold, 56–71 (1984).

13. Hahn, G.T. and Rosenfield, A.R., "Local Yielding and Extension of a Crack Under Plane Stress," Acta Metall., **13**, *293–306 (1965).*

14. Yang, W. and Freund, L.G., "Transverse Shear Effects for Through-cracks in an Elastic Plate," Int. J. Solids Struct., **21**, *977–994 (1985).*

15. Nakamura, T. and Parks, D.M., "Three-dimensional Stress Field near the Crack Front of Thin Elastic Plate," J. Appl. Mech., **55**, *805–813 (1988).*

16. Rosakis, A.J. and Ravi-Chandar, K., "On Crack-tip Stress State: An Experimental Evaluation of Three-dimensional Effects," Int. J. Solids Struct., **22**, *121–134 (1986).*

17. Sagnac, G., "L'ether lumineux demontre par l'effect du vent relatif dether dans un interferometre en rotation uniforme," Acadamie der Sciences, Paris Comptes Randus, **157**, *708–710 (1913).*

18. Eichmann, G., Li, Y., and Alfano, R.R., "Digital Optical Logic Using a Pulsed Sagnac Interferometer Switch," Opt. Eng., **25**, *91–97 (1986).*

19. Huang, A., "Sagnac Fiber Logic Gates and Their Possible Applications: A System Perspective," Appl. Opt., **33**, *6254–6266 (1994).*

20. Post, D., "Moire Interferometry," in Handbook on Experimental Mechanics, 2d ed., A.S. Kobayashi, ed., Society for Experimental Mechanics, Bethel, CT, 297–364 (1993).

21. Wang, F.X., Kang, B.S.-J., and Lin, K.Y., "Full-field Displacements by Four-beam Moire Interferometry," SEM Spring Conference on Experimental Mechanics, Milwaukee, Wisconsin, 278–284 (1991).

22. Hertzberg, R.W., Elements of Fracture Mechanics, John Wiley & Sons, New York (1989).

23. Hellen, T.K., "On the Method of Virtual Crack Extension," Int. J. Numer. Meth. Eng., **9**, *187–207 (1975).*

24. Parks, D.M., "A Stiffness Derivative Finite Element Technique for Determination of Elastic Crack-tip Stress Intensity Factors," Int. J. Fract., **10**, *487–502 (1974).*

25. Barbero, E.J., "Computer Code for 2-D and 3-D Jacobian Derivative Method," CFC report, West Virginia University, Morgantown (1995).

26. Tada, H., Paris, P.C., and Irwin, G.R., The Stress Analysis of Cracks—Handbook, Paris Production, Inc., St. Louis, MO (1985).